

PointNeuron: 3D Neuron Reconstruction via Geometry and Topology Learning of Point Clouds

Runkai Zhao

University of Sydney

rzha9419@uni.sydney.edu.au

Heng Wang

University of Sydney

hwan9147@uni.sydney.edu.au

Chaoyi Zhang

University of Sydney

czha5168@uni.sydney.edu.au

Weidong Cai

University of Sydney

tom.cai@sydney.edu.au

Abstract

Digital neuron reconstruction from 3D microscopy images is an essential technique for investigating brain connectomics and neuron morphology. Existing reconstruction frameworks use convolution-based segmentation networks to partition the neuron from noisy backgrounds before applying the tracing algorithm. The tracing results are sensitive to the raw image quality and segmentation accuracy. In this paper, we propose a novel framework for 3D neuron reconstruction. Our key idea is to use the geometric representation power of the point cloud to better explore the intrinsic structural information of neurons. Our proposed framework adopts one graph convolutional network to predict the neural skeleton points and another one to produce the connectivity of these points. We finally generate the target SWC file through interpretation of the predicted point coordinates, radius, and connections. Evaluated on the *Janelia-Fly* dataset from the *BigNeuron* project, we show that our framework achieves competitive neuron reconstruction performance. Our geometry and topology learning of point clouds could further benefit 3D medical image analysis, such as cardiac surface reconstruction. Our code is available at <https://github.com/RunkaiZhao/PointNeuron>.

1. Introduction

Neuron morphology plays an essential role in the analysis of brain functionality. Digital 3D neuron reconstruction, also named 3D neuron tracing, is a computer-aided process to extract the anatomical structure and connectivity of neuron circuits from the volumetric microscopy image. Acquisitions of neuron morphology models in the past several decades have relied on manual annotation from neuroscientists. Due to the diversity and complexity of neuron

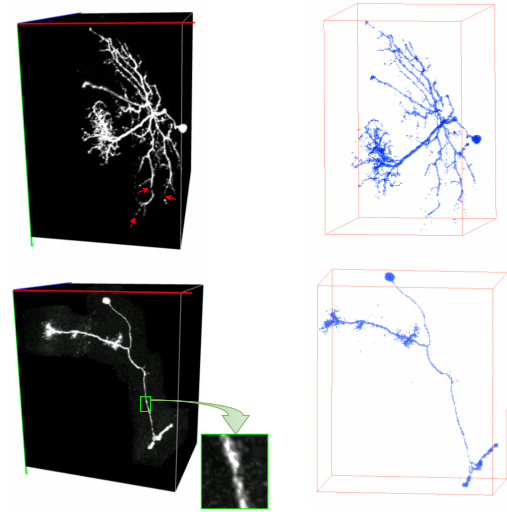


Figure 1: We re-think the structural representation of neuron by using point cloud. Left: the voxel-wise neuron microscopy image; Right: the point-wise neuron after the format transformation. Due to the limits of optical microscope imaging, there are gaps along neuron tree-like arbors (red arrows), and the neuron structure is surrounded by the background noises (green box). Note voxel-based representation is inherently dense in three dimensions while our point-based one is more efficient in memory (e.g., $200 \times 100 \times 150$ voxels versus 4500 points).

morphology, the manual annotation work is extremely time-consuming and labor-intensive. The manual annotations are recorded as SWC files for digitally storing the neuron morphologies which use a set of connected points to constitute the hierarchical neuronal trees. It includes the identity of each neuron node, such as ID, type, position, radius, and parent ID. Recently, many researchers have devoted more

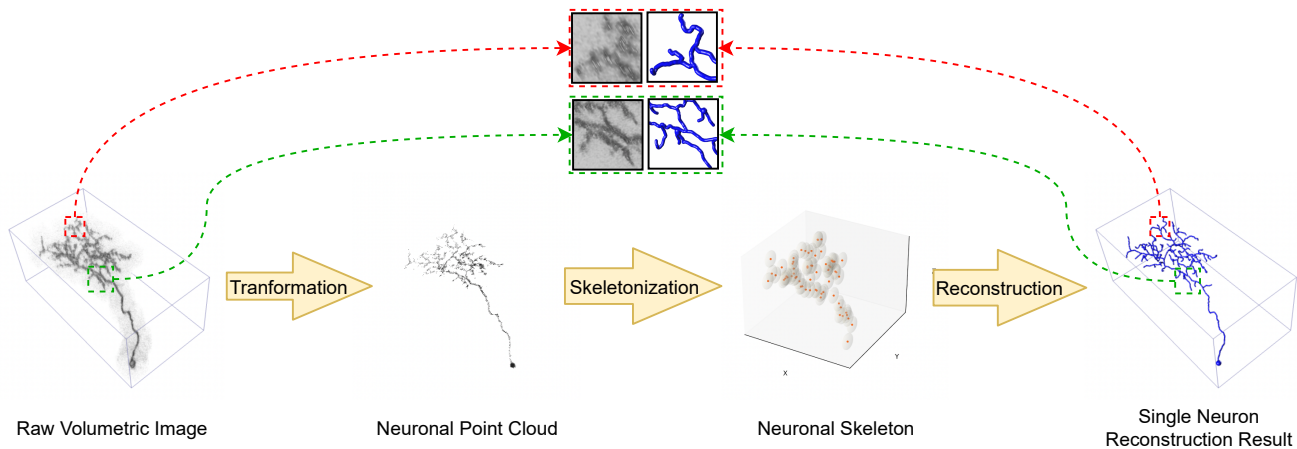


Figure 2: The main procedures of our proposed method, *PointNeuron*, for neuron reconstruction from a volumetric microscopy image. The green and red boxes highlight parts of our reconstruction improvements.

attention to completing neuron reconstruction in an automatic or semi-automatic manner. The BigNeuron challenge [34] and the DIADEM challenge [6] have been hosted to develop automatic tracing algorithms by providing a sizeable single neuron morphology database and open-source software tools for neuroscience studies.

Early digital neuron reconstruction algorithms relied on sophisticated mathematical models, which can be categorized into global and local algorithms. The global approaches, such as open-curve snake [48], APP [35], APP2 [51], FMST [52], and others [24, 33, 40, 17, 38, 45], consist of multiple stages which are pre-processing to denoise the raw image, tree-like structure initialization, and post-processing to refine the reconstructed traces. The local approaches [55, 3, 12] are to trace the neuronal tree from the seed point location with manual intervention or automatic detection.

Nevertheless, reconstructing neuron morphologies from microscopy images are still error-prone especially when given low-quality neuron image data. Due to the inhomogeneous fluorescence illumination and inherent light microscopy imaging limits, the raw neuron image stacks are often contaminated by numerous background noises. In addition, the voxels in dendrite and branch termini have a much lower intensity than those in soma and axon regions, which results in discontinuous neuron branches and impedes predicting the intact connections of neuron circuits. These two challenges are highlighted in the two neuron examples of Figure 1. Lastly, since the 3D neuron images in the BigNeuron dataset are obtained from worldwide research laboratories and light microscopy measurements are varied, the exhibited neuron morphologies are diverse and complex.

Various deep learning techniques have been success-

fully applied in medical image processing [37, 32, 15, 14, 21], which has inspired researchers to utilize the hierarchical feature learning ability of convolution-based models to solve the challenging neuron reconstruction problem [26, 42]. In order to identify the neuron structures from a larger receptive field, recent works focus on introducing global contextual features into the convolution-based segmentation work, such as inception learning module [26], multi-scale kernel fusion [46], Atrous Spatial Pyramid Pooling (ASPP) [25], and graph reasoning module [43].

In this paper, we re-think the spatial representation of neuron morphology. Rather than following the traditional 3D volumetric representation, we propose to explicitly leverage the sparsely organized point clouds to represent neuronal arbours and dendrites. As shown in Figure 1, we transform the voxels of original 3D neuron images into points, then reformulate this reconstruction task to predict the geometric and topological properties for the points in cartesian coordinate system. We design a novel framework, named *PointNeuron*, to extract neuronal structures from these point cloud data. Specifically, our framework consists of two major stages. The first stage is to extract a succinct neuron skeleton from the noisy input points and formulate the geometric feature. The connectivity among the unordered points is predicted at the second stage. The general idea of our method is stated in Figure 2. Our key contributions are summarized as follows: 1) we propose to describe the neuron circuits in point format for better understanding of the spatial information in 3D space, instead of original volumetric image stacks; 2) we present a novel pipeline, *PointNeuron*, as an automatic 3D neuron reconstruction method by learning the characterization of point clouds, which can be generalized to improve reconstruction performance of all tracing algorithms; and 3) we present

the point-based module to effectively capture the geometry information for generating the compact neuron skeletonization.

2. Related Works

Traditional neuron reconstruction algorithms consist of three main steps: pre-processing the raw 3D microscopy image stacks, initializing the tree-like neuronal graph map, and then pruning the reconstruction map until the compact result is obtained. APP [35] and APP2 [51] cover all the potential neuron signals on the raw image input for the initial reconstruction map and remove the surplus neuron branches for a compact structure at the pruning step. Like the APP family, FMST [52] applies the fast marching algorithm with edge weights to initialize neuron traces and prunes them based on the coverage ratio of two intersected neuron nodes. NeuTube [16] implements free editing functions and the multi-branch tracing algorithm from seed source points. Reversely, Rivulet [54] and Rivulet2 [29] capture the neuron traces from the furthest branch termini to the seed point. LCMBBoost [20] and SmartTracing [8] incorporate the deep learning-based modules into an automatic tracing algorithm without human intervention.

With the emergence of 3D U-Net [13] showing great success in medical image segmentation tasks, learning-based segmentation prior to applying the tracing algorithm is able to highlight the neuron signal and enhance the input neuron image quality. Some advanced deep learning techniques are applied to improve the image segmentation performance, such as inception learning module [26], multi-scale kernel fusion [46], atrous convolution [9], and Atrous Spatial Pyramid Pooling (ASPP) [10, 25]. [43, 41] incorporate graph reasoning module to the multi-scale encoder-decoder network for eliminating the semantic gap of image feature learning. For computational saving and faster inference, [47] proposes a light-weighted student inference model guided by the more complex teacher model via knowledge distillation. To handle the small-size neuron dataset, [44] improves neuron image segmentation performance through the VCV-RL module extracting intra- and inter-volume voxels of same semantics into the latent space. [39] builds a GAN-based framework to synthesize neuron training images from the manually annotated skeletons.

As the deep learning advances in medical image analysis, researchers have raised the interests to analyze 3D medical images by applying deep learning techniques. Although the existing works process medical images in voxel-wise representation, an increasing number of researchers are studying the 3D structures with the insight of point clouds. They leverage the 3D point cloud representation to learn more discriminative object features for different medical image tasks [53], such as cardiac mesh reconstruction [11], volumetric segmentation [23, 2], and vessel centerline

extraction [22]. For example, [23, 22, 2] use the characterization of point clouds to learn the global context feature for enhancing the CNN-based image segmentation performance. Also, [1] and [4] take into account the anatomical properties of streamline and mesh structure in the form of point cloud representation.

The great success of introducing point cloud concepts into the domain of medical image analysis and the fact that existing tracing methods have not considered the usage of the point cloud encourage us to address the challenging neuron reconstruction task from a novel perspective. We aim to improve 3D neuron reconstruction performance through the powerful geometric and topological representation of point clouds. Therefore, we shift one of the most challenging medical image tasks to the scope of point clouds.

3. Method

We propose a novel pipeline, *PointNeuron*, to perform 3D neuron morphology reconstruction in the point-based manner. Given the voxel-wise neuron image input, we initially convert it to a point cloud in Section 3.1. Then we forward the neuron point cloud into the Skeleton Prediction module to generate a series of neuron skeletal points in Section 3.2. After that, we design the Connectivity Prediction module to link these skeletal points through analyzing the node relationships of graph data structure in Section 3.3. Lastly, we present the specific training losses in Section 3.4. Our pipeline is shown in Figure 3.

3.1. Voxel-to-Point Transformation

Given a raw volumetric neuron image of size $\mathbb{R}^{H \times W \times D}$, a thresholding value θ is pre-defined to segment the neuron structure and remove a majority of noises. Every voxel with an intensity larger than θ is positioned and transformed to a point. To handle large amount of points, we split all the neuron points into K patches. Hence, the neuron point input can be represented as $\mathcal{P} = K \times \{p_i : [x_i; I_i]\}_{i=1}^{N_p}$ where N_p is the number of points per patch with the Cartesian coordinate $x_i \in \mathbb{R}^3$ and the intensity $I_i \in \mathbb{R}$.

3.2. Neuron Skeleton Prediction

In this module, we extract N_s skeletal points from the neuronal point cloud input to constitute a neuron skeleton with the point-wise F -dimensional geometric features. There are three primary steps: learning the deep geometric features of neuron points through a graph-based encoder, generating the center proposals at local regions, and producing the compact neuron skeleton.

Point cloud geometry learning. Since the point clouds representing neuron structures are uneven and unordered in coordinate space, they cannot be simply processed by a regular grided convolution kernel like typical pixel- or

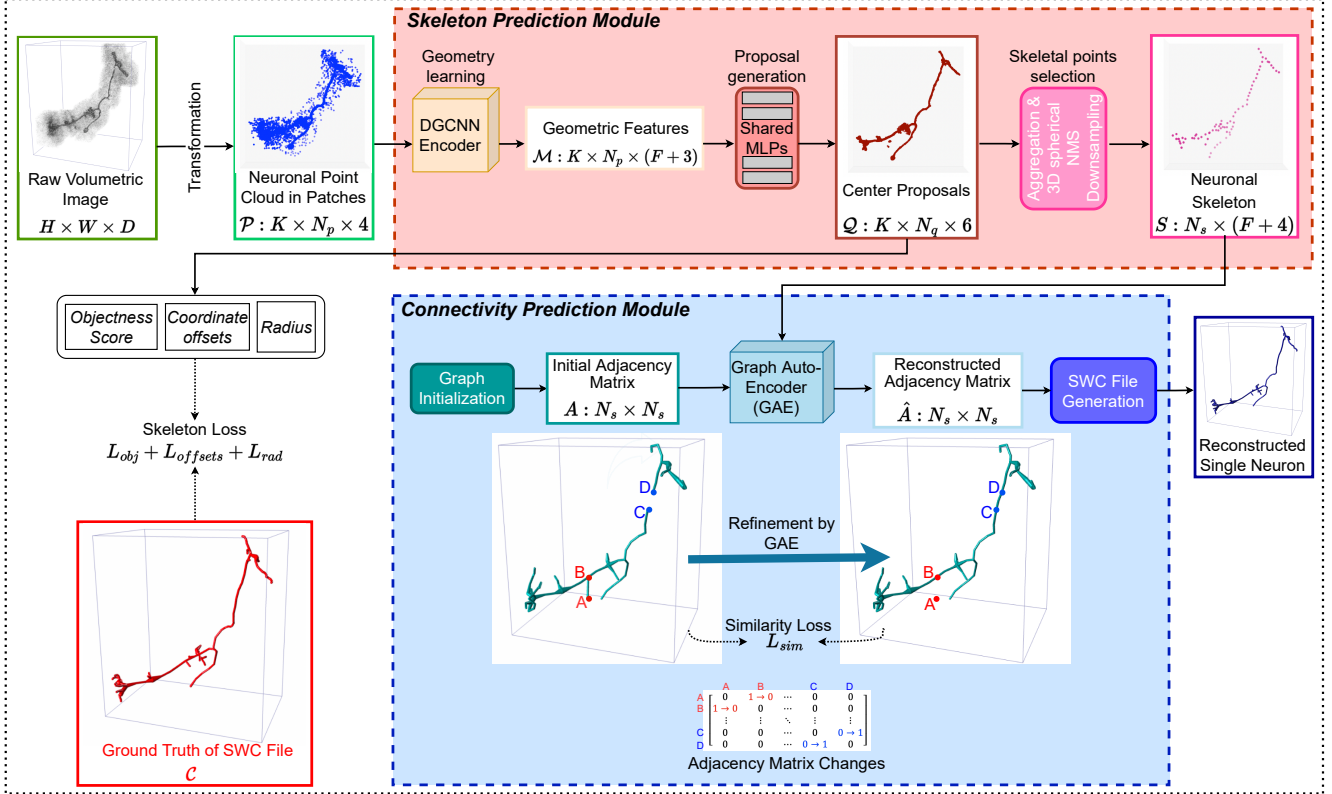


Figure 3: The overview of our proposed pipeline, *PointNeuron*. The neuron voxels are initially transformed to point clouds. Then a DGCNN encoder [49] is applied to learn deep geometric features on the neuron points. These features are processed via a proposal generation step to predict center proposals with Euclidean coordinate offsets, objectness score, and radius. To obtain a compact neuronal skeleton, we apply aggregation and 3D NMS downsampling to select the neuron skeletal points. Sequentially, we link these neuron skeletal points to produce neuron connectivity. Given the initial adjacency matrix and geometric skeleton features, we apply a graph auto-encoder to compute the correlations among points and reconstruct the adjacency matrix. After the refinement process of removing the spurs (labeled by **A** and **B** points) and bridging the gaps (labeled by **C** and **D** points), the final neuron reconstruction result is recorded in an SWC file. The skeleton loss and the similarity loss supervise the training process of skeleton and connectivity prediction, respectively.

voxel-wise images. Therefore, we adopt DGCNN [49] as our encoder to learn the spatial characteristics of neuron point clouds. The EdgeConv blocks in this architecture are designed to encode the local point-wise semantic feature, which connects a neuron point with its k -nearest neighboring points then computes and fuses edge features by graph reasoning. This local aggregation could be beneficial in complimenting topological information to neuron points. Additionally, DGCNN can yield hierarchical geometric features and incorporate multi-scale contextual information as the node relationships are dynamically refreshed after each layer. DGCNN encoder, stacking several EdgeConv blocks with residual connections, takes input points \mathcal{P} , and outputs the geometric features $\mathcal{M} \in \mathbb{R}^{K \times N_p \times (F+3)}$ where F is the feature dimension. The Cartesian coordinates of points are remained the same.

Proposal generation. We observe that the ground truth SWC file uses a set of key points to denote a single neuron as a hierarchical tree-like model, which constitutes a neuron skeleton, while each of key points could be considered as the center of its near neuron points at local region. The key points of SWC file are represented as $\mathcal{C} = \{c_j : [y_j; r_j^c]\}_{j=1}^{N_c}$ where N_c is the number of SWC key points with the coordinate $y_j \in \mathbb{R}^3$ and radius $r_j^c \in \mathbb{R}$. Inspired by this, we move the neuron point toward its nearest local center by the coordinate offsets $\Delta d_i \in \mathbb{R}^3$, which is schematically illustrated in Figure 4. It is expected that the neuron points are pushed close to the center of local region and the sparse neuron point cloud becomes more concentrated as shown in Figure 5. Consequently, we consider these moved neuron points as the center proposals \mathcal{Q} . In our implementation, the learned geometric features of input points are forwarded into the

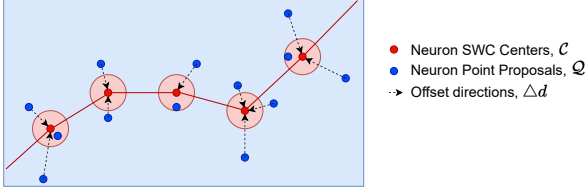


Figure 4: The surrounding points are moving toward the neuron centers defined in the SWC files by the predicted offsets. The offsets are supervised by the distance-based losses.

proposal module of a shared multi-layer perceptron (MLP). The MLP comprises of fully-connected layers, batch normalization, and LeakyReLU. The proposal module predicts the center proposals $\mathcal{Q} = \{q_i : [\tilde{x}_i; \hat{s}_i; \hat{r}_i^q]\}_{i=1}^{N_q}$ with the coordinate $\tilde{x}_i \in \mathbb{R}^3$, the objectness score $\hat{s}_i \in \mathbb{R}^2$ (we formulate the objectness score prediction as a binary classification problem supervised by a cross entropy loss), and the radius $\hat{r}_i^q \in \mathbb{R}$ are generated. The coordinate of a center proposal is obtained by adding the coordinate offsets to the input point, $\tilde{x}_i = x_i + \Delta d_i$.

Skeletal points selection. We aim to select the high-confidence center proposals as the neuron skeletal points from the abundant and overlapped center proposals. We thus resort to a spherical NMS downsampling strategy with the 3D geometric information predicted by proposal generation to obtain a compact neuron skeleton \mathcal{S} . Non-max suppression (NMS) [5, 28, 19, 18] is a general computer vision approach to selecting one object out of several overlapped objects. The core of this approach is to eliminate redundant object proposals through iteratively comparing the confidence score and the intersection over union (IoU) among proposals. Following this idea, we initially use the predicted Cartesian coordinates and radii of center proposals to form the potential skeletal spheres. We store the center proposals with the highest objectness score per iteration as output while discarding the remaining skeletal sphere if the IoU of spherical volume with this output is greater than a threshold θ_{IoU} . This method can effectively take the neuron skeletal points out of the center proposals. It is clearly visualized in Figure 5 that these representative skeletal points constitute a succinct neuron skeleton and the neuron structural morphology is more prominently reflected than neuron input points and center proposals.

3.3. Neuron Connectivity Prediction

In this section, inspired by the mesh generation of Point2Skeleton [27], we encode the connectivity of a neuron circuit as a graph data structure. The graph is a high freedom degree structure consisting of nodes and edges. The neuron skeletal spheres are the graph nodes, and the parent-child relationship between the two points is the edge

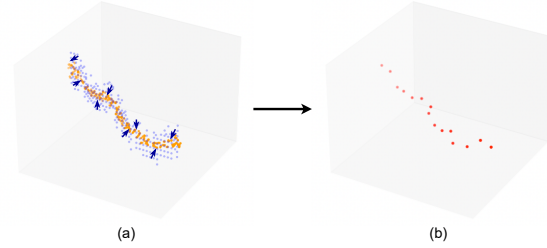


Figure 5: Visualization of the neuron skeleton prediction process for a small neuron branch: (a) the raw neuron points (blue) are adaptively directed into the structure interior, then generating the preliminary neuron center proposals (orange); (b) the sampled skeletal points (red) are obtained to represent more clear neuron morphology.

of two graph nodes.

Graph initialization. During training, we extract the point-wise relationships from the ground truth SWC file to generate a preliminary parent-child relationship of neuron points. The graph initialization is based on these preliminary relationships, which demonstrates basic connectivity information of the neuronal skeleton and ensures a relatively reliable topology. The reconstructed graph map is expected to be as much similar to the initialized graph as possible. Different graph initialization strategies for inference will be discussed later.

Connectivity prediction from the reconstructed graph map. According to this topology information, the initial undirected graph $A = (\mathcal{V}, \mathcal{E})$ is formed where \mathcal{V} is the set of neuron skeletal points and \mathcal{E} is the set of edges. The adjacency matrix A as one input to the Graph Auto-Encoder (GAE) encodes the edge connectivity. To effectively utilize the meaningful geometry information from the skeleton prediction module, we concatenate the geometric contextual features of the neuron skeletal points M , the Cartesian coordinates \tilde{x} , and their radii \hat{r}^q to establish the node features $X \in \mathbb{R}^{N_s \times (F+4)}$ where N_s is the number of neuron skeletal points. The encoder part of GAE is a stack of graph convolution layers of graph convolution, batch normalization, and ReLU, which compresses the node feature into the latent embedding Z :

$$Z = GCN(X, A). \quad (1)$$

The decoder part of GAE adopts the inner product to reconstruct the new adjacency matrix \hat{A} :

$$\hat{A} = Z \cdot Z^T. \quad (2)$$

SWC file generation. Finally, we design a recursive method to interpret the predictions of neuron skeletal points and the reconstructed connectivity. It can recursively search

the detected neuron points and edges to rebuild the target SWC file.

3.4. Learning Objectives

For neuron skeleton prediction, we expect that our predicted skeleton reflects the identical structural meaning as the key points manually annotated in the SWC file.

Coordinate offset loss. The bi-directional Chamfer Distance (CD) is measured between the SWC key points and center proposals to optimize the predicted coordinate offsets:

$$L_{offsets} = \sum_{a \in \{y_j\}} \min_{b \in \{\hat{x}_i\}} \|a - b\|_2^2 + \sum_{b \in \{\hat{x}_i\}} \min_{a \in \{y_j\}} \|b - a\|_2^2. \quad (3)$$

Objectness loss. In addition to explicitly directing the points, we introduce a cross-entropy loss to supervise the predicted objectness score indicating how confident a local center proposal locates inside of the neurite region:

$$L_{obj} = -\frac{1}{N_p} \sum_i s_i \log(\sigma(\hat{s}_i)) + (1 - s_i) \log(1 - \sigma(\hat{s}_i)), \quad (4)$$

where \hat{s}_i is the objectness score prediction, s_i is the objectness label, and σ is the Sigmoid activation function. We assign the center proposals entered into the ground truth SWC sphere to have true objectness labels and the others to have false objectness labels. These two complementary loss functions encourage the consistency of the predicted neuron center proposals and ground truth SWC points from two perspectives of Euclidean geometry and object confidence, which are discussed in Section 4.4 - Ablation Study.

Radius loss. The radius of a neuron point is supposed to be the same as the radius of the nearest center. We use Mean Absolute Error (MAE) to calculate the radius loss:

$$L_{rad} = \frac{1}{N_p} \sum_i |\xi(\mathcal{C}, q_i) - \hat{r}_i^q|, \quad (5)$$

where $\xi(\mathcal{C}, q_i)$ represents the radius of the nearest SWC point to the center proposal q_i .

These three losses are summed with weight λ to supervise the skeleton prediction module:

$$L_{skel} = L_{offsets} + \lambda L_{obj} + L_{rad}. \quad (6)$$

When training the neuron connectivity prediction module, we aim to make the reconstructed adjacency matrix as similar as possible to the input adjacency matrix initialized by the SWC file.

Similarity loss. We apply a masked cross entropy loss to supervise GAE learning:

$$L_{sim} = \frac{1}{N_s} (M \odot (A \log(\sigma(\hat{A})) - (1 - A) \log(\sigma(1 - \hat{A})))), \quad (7)$$

where M is the mask of the interested points, and σ is the Sigmoid activation function.

4. Experiments and Results

4.1. Dataset and Implementation Details

Dataset. Our proposed framework is evaluated on the Janelia-Fly dataset of the BigNeuron project, which features diverse neuron morphologies of the fruitfly on cortical and subcortical areas, retina, and peripheral nervous system regions [31]. The volumetric images of this dataset were imaged from light microscopy, and their manual annotations were processed by the Brainbow method [30]. We separate the total 42 images into 35 training images, 3 validation images, and 4 testing images. The average resolutions for training and testing images are $197 \times 198 \times 168$ and $262 \times 159 \times 181$. The foreground neuron voxels are segmented out by intensity thresholding (of $\theta = 0.2$). By mapping these foreground voxels into points in Cartesian space, we obtain around $N = 12000$ points per image. The number of points per image in this task is much larger than the number of point clouds for normal instances in ModelNet40 [50] and ShapeNet [7]. A point cloud patch of $N_p = 512$ is randomly cropped from the entire neuronal points as the input points for training our proposed framework, and data augmentation is applied including rotation and flipping.

Table 1: Quantitative comparisons with traditional algorithms for neuron reconstruction performance.

Method	ESA ↓	DSA ↓	PDS ↓	Precision (%) ↑	Recall (%) ↑	F1 (%) ↑
APP2	3.22±0.38	7.22±0.89	0.32±0.05	64.51±9.84	51.67±21.94	52.63±13.22
+ 3D U-Net [13]	1.59±0.19	3.66±0.81	0.22±0.02	86.23±7.76	56.30±19.39	64.92±15.33
+ 3D MKF-Net [46]	1.62±0.21	3.85±0.76	0.22±0.03	89.03±8.74	55.07±18.13	65.15±1.93
+ VCV-RL (SOTA) [44]	1.52±0.21	3.48 ±0.29	0.21±0.22	87.25±7.41	56.87±17.92	66.17±14.39
+ PointNeuron (Proposed)	1.43 ±0.29	4.13±0.85	0.18 ±0.03	91.56 ±6.81	63.17 ±22.85	71.7 ±17.48
NeuTube [16]	2.05±0.66	5.58±1.37	0.26±0.08	87.75±8.55	52.11±15.90	62.89±12.58
+ PointNeuron (Proposed)	2.03 ±0.87	5.33 ±1.7	0.23 ±0.06	93.13 ±6.33	52.55 ±14.9	65.26 ±12.15
LCMboost-FastMarching [20]	1.96±0.72	4.85±1.52	0.23±0.08	85.04±9.11	44.92±18.55	55.86±16.57
+ PointNeuron (Proposed)	1.76 ±0.63	4.79 ±1.38	0.18 ±0.05	93.31 ±6.85	50.87 ±21.35	63.03 ±19.55

Network architecture details. We stack 3 EdgeConv blocks in DGCNN to encode the geometric contextual information, then the geometric features are processed by the proposal module of 3 shared MLP layers to generate center proposals. For connectivity prediction, GAE of 12 layers with residual learning is used. More details are provided in the supplementary material.

Training the network. The neuron skeleton prediction and neuron connectivity prediction modules are separately trained with Adam optimizer. For skeleton prediction module, the backbone DGCNN network and proposal module are employed together to generate center proposals, which are trained with L_{skel} (with $\lambda = 10$) and a learning rate $1e^{-3}$. 3D spherical NMS with the acceptable range

of θ_{IoU} is from 0.05 to 0.25 is to select high-confidence center proposals for obtaining a compact neuron skeleton. When training connectivity prediction module, we freeze the skeleton prediction module and train the GAE with L_{sim} and a learning rate of $5e^{-4}$. Training these two modules to convergence on GeForce RTX 2080 Ti takes 1200 and 200 epochs, respectively.

Inference. Our proposed skeleton prediction module predicts partial neuron skeleton from a window sliding along the neuron structure. Then, these outputs are aggregated to formulate the complete skeleton. Afterwards, linking the neuron skeletal nodes explores the neuronal relationships and outputs the final neuron reconstruction as a new SWC file in connectivity prediction module.

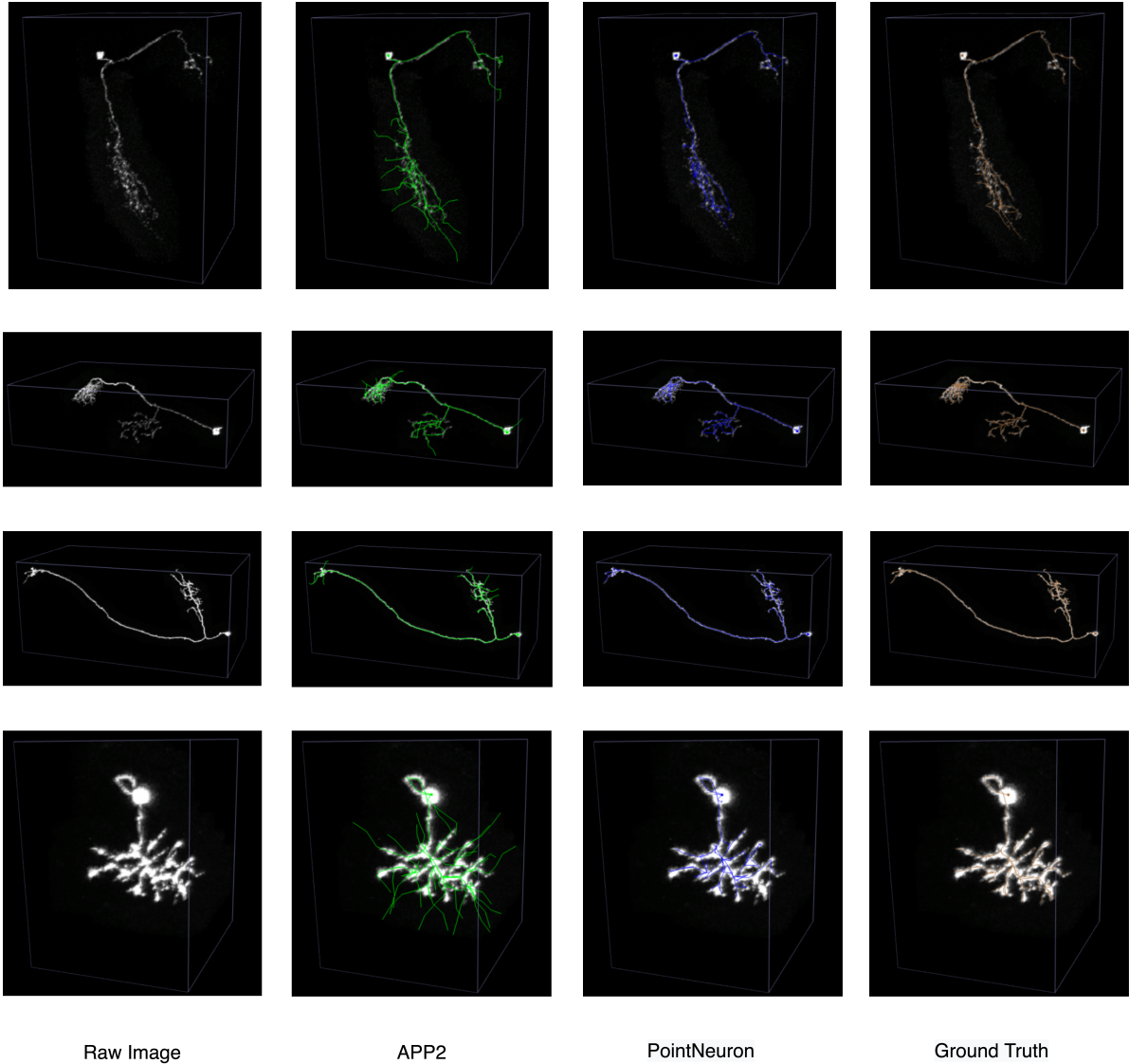


Figure 6: Visualization of the neuron tracing performance comparisons on test. Each row represents one image.

4.2. Results and Analysis

We use the three spatial distance-driven metrics proposed by [36], Entie Structure Average (ESA), Different Structure Average (DSA), and Percentage of Different Structure (PDS), to measure the geometric discrepancy between the neuron reconstruction and the ground truth SWC file. The calculation of these three metrics takes into account the correctness of connectivity of neuron nodes, which is processed by the Vaa3D software plugin. We report the reconstruction performance using Precision, Recall, and F1, where true positive (TP), false positive (FP), and false negative (FN) are determined by measuring how far a predicted neuron point is away from the nearest ground truth points.

The quantitative evaluations of our proposed method and traditional tracing algorithms are shown in Table 1. Aiming to facilitate comparisons with traditional algorithms and emphasize the performance improvements from our method, “+” means that the previous neuron tracing algorithms (APP2, NeuTube, and LCMboots) were used for graph initialization of the connectivity prediction module of our proposed framework. As indicated in Table 1, the tracing performance with our proposed method is better than the traditional algorithms. Based on the same APP2, our proposed method outperforms the previous deep voxel-based models and is comparable to the SOTA work of VCV-RL [44]. We present a visualization comparison of reconstructions with APP2 and ours in Figure 6. The predicted neuron structures achieve a better match to the ground truth spatially, and most neuron skeletal nodes are considered to be structurally meaningful. It is noticeable that the reconstruction results from our method produce less false positive points (or branches) than APP2 and are closer to the ground truth.

4.3. Model Complexity

We measure the complexity of our proposed point-based model with comparisons to the previous deep learning voxel-based models. Table 2 shows the remarkable advantages of our point-based model in terms of computational memory take-up and inference speed. With the input data type as point cloud, we eliminate the computing memory need for the majority of senseless background voxels on a volumetric microscopy image and reduce the input memory size by 95.6%. In addition, our proposed MLP-dominated model requires fewer trainable parameters than convolution-based networks, while being much more efficient in the inference procedure.

4.4. Ablation Study

We conduct an ablation study as listed in Table 3. Models 1 and 2 are configured with different losses, demonstrating that the offsets loss $L_{offsets}$ effectively pushes the neuron

Table 2: Model complexity analysis of our point-based model with previous voxel-based models for one pass inference.

Model	Input memory size (MB)	Params (M)	Inference time (ms)
3D U-Net	33.55	1.50	917.38
3D MKF-Net	33.55	1.55	925.69
VCV-RL	33.55	1.53	1038.67
Proposed	1.47	1.17	665.34

points inward, but a single geometric loss cannot reach the optimal result. In Model 3, the encoder in skeleton prediction is replaced with another point-based backbone, PointNet++, and it does not perform as efficiently as DGCNN, given that DGCNN employs a dynamic design to construct the graph map in each layer which is superior for learning global representative features in latent space. We also attempt to directly forward the plain point feature of Cartesian coordinate and intensity into the GAE in the connectivity prediction module, and the results of Model 4 illustrate that the geometric information of neuronal points learned from the skeleton prediction module is essential to generating accurate links between neuron points. Furthermore, we test different downsampling methods. Our proposed spherical NMS downsampling outperforms the regular FPS and uniform sampling. The reason is that it takes into account the local geometric structure, and its principle is suited to handling the unevenness of the point cloud.

Table 3: Quantitative ablation studies with different configurations.

ID	Method	ESA↓	DSA↓	PDS↓	F1 score (%)↑
1	w/o L_{obj}	1.61±0.20	4.71±0.73	0.20±0.03	70.37±17.87
2	w/o $L_{offsets}$	1.70±0.17	4.74±0.61	0.22±0.2	70.83±18.17
3	PointNet++	1.50±0.33	4.28±0.99	0.19±0.04	70.96±17.76
4	w/o DGCNN	5.06±2.07	6.89±2.36	0.38±0.06	58±34.32
5	FPS downsampling	1.46±0.31	4.15±0.73	0.19±0.04	68.67±18.84
6	Uniform downsampling	1.51±0.28	4.19±0.67	0.20±0.03	68.65±18.83
7	Proposed	1.43±0.29	4.13±0.85	0.18±0.03	71.7±17.48

5. Conclusion

In this paper, we propose to represent neuron structures with point cloud data and design a novel point-based pipeline, *PointNeuron*, to solve the challenging problem of automatic 3D neuron reconstruction. Taking transformed neuron point clouds as input, a skeleton prediction module is designed to obtain the neuronal skeletons, after which a connectivity prediction module learns the linkage among skeletal points and produce the final reconstructions. Experiments show that our point-based approach is more efficient and able to achieve finer reconstruction results compared to those based on traditional 3D volumetric data, which should facilitate 3D medical analysis and point-cloud-driven healthcare applications.

References

- [1] Pietro Astolfi, Ruben Verhagen, Laurent Petit, Emanuele Olivetti, Jonathan Masci, Davide Boscaini, and Paolo Avesani. Tractogram Filtering of Anatomically Non-plausible Fibers with Geometric Deep Learning. In *International Conference on Medical Image Computing and Computer-Assisted Intervention (MICCAI)*, pages 291–301. Springer, 2020.
- [2] Fabian Balsiger, Yannick Soom, Olivier Scheidegger, and Mauricio Reyes. Learning Shape Representation on Sparse Point Clouds for Volumetric Image Segmentation. In *International Conference on Medical Image Computing and Computer-Assisted Intervention (MICCAI)*, pages 273–281. Springer, 2019.
- [3] Erhan Bas and Deniz Erdogmus. Principal Curves as Skeletons of Tubular Objects. *Neuroinformatics*, 9(2):181–191, 2011.
- [4] Žiga Bizjak, Boštjan Likar, Franjo Pernuš, and Žiga Špiclin. Vascular surface segmentation for intracranial aneurysm isolation and quantification. In *International Conference on Medical Image Computing and Computer-Assisted Intervention (MICCAI)*, pages 128–137. Springer, 2020.
- [5] Navaneeth Bodla, Bharat Singh, Rama Chellappa, and Larry S Davis. Soft-NMS—Improving Object Detection With One Line of Code. In *Proceedings of the IEEE International Conference on Computer Vision (ICCV)*, pages 5561–5569, 2017.
- [6] Kerry M Brown, Germán Barrionuevo, Alison J Canty, Vincenzo De Paola, Judith A Hirsch, Gregory S X E Jefferis, Ju Lu, Marjolein Snippe, Izumi Sugihara, and Giorgio A Ascoli. The DIADEM Data Sets: Representative Light Microscopy Images of Neuronal Morphology to Advance Automation of Digital Reconstructions. *Neuroinformatics*, 9(2):143–157, 2011.
- [7] Angel X Chang, Thomas Funkhouser, Leonidas Guibas, Pat Hanrahan, Qixing Huang, Zimo Li, Silvio Savarese, Manolis Savva, Shuran Song, Hao Su, et al. ShapeNet: An information-rich 3D model repository. *arXiv preprint arXiv:1512.03012*, 2015.
- [8] Hanbo Chen, Hang Xiao, Tianming Liu, and Hanchuan Peng. SmartTracing: self-learning-based Neuron reconstruction. *Brain Informatics*, 2(3):135–144, 2015.
- [9] Liang-Chieh Chen, George Papandreou, Iasonas Kokkinos, Kevin Murphy, and Alan L Yuille. DeepLab: Semantic Image Segmentation with Deep Convolutional Nets, Atrous Convolution, and Fully Connected CRFs. *IEEE Transactions on Pattern Analysis and Machine Intelligence (TPAMI)*, 40(4):834–848, 2017.
- [10] Liang-Chieh Chen, Yukun Zhu, George Papandreou, Florian Schroff, and Hartwig Adam. Encoder-Decoder with Atrous Separable Convolution for Semantic Image Segmentation. In *Proceedings of the European Conference on Computer Vision (ECCV)*, pages 801–818, 2018.
- [11] Xiang Chen, Nishant Ravikumar, Yan Xia, Rahman Attar, Andres Diaz-Pinto, Stefan K Piechnik, Stefan Neubauer, Steffen E Petersen, and Alejandro F Frangi. Shape registration with learned deformations for 3D shape reconstruction from sparse and incomplete point clouds. *Medical Image Analysis*, 74:102228, 2021.
- [12] Anna Choromanska, Shih-Fu Chang, and Rafael Yuste. Automatic reconstruction of neural morphologies with multi-scale tracking. *Frontiers in Neural Circuits*, 6:25, 2012.
- [13] Özgün Çiçek, Ahmed Abdulkadir, Soeren S Lienkamp, Thomas Brox, and Olaf Ronneberger. 3D U-Net: Learning Dense Volumetric Segmentation from Sparse Annotation. In *International Conference on Medical Image Computing and Computer-Assisted Intervention (MICCAI)*, pages 424–432. Springer, 2016.
- [14] Qi Dou, Hao Chen, Yueming Jin, Lequan Yu, Jing Qin, and Pheng-Ann Heng. 3D Deeply Supervised Network for Automatic Liver Segmentation from CT Volumes. In *International Conference on Medical Image Computing and Computer-Assisted Intervention (MICCAI)*, pages 149–157. Springer, 2016.
- [15] Michal Drozdal, Eugene Vorontsov, Gabriel Chartrand, Samuel Kadoury, and Chris Pal. The Importance of Skip Connections in Biomedical Image Segmentation. In *Deep Learning and Data Labeling for Medical Applications*, pages 179–187. Springer, 2016.
- [16] Linqing Feng, Ting Zhao, and Jinhyun Kim. neuTube 1.0: A New Design for Efficient Neuron Reconstruction Software Based on the SWC Format. *eNeuro*, 2(1), 2015.
- [17] Rohan Gala, Julio Chapeton, Jayant Jitesh, Chintan Bhavsar, and Armen Stepanyants. Active learning of neuron morphology for accurate automated tracing of neurites. *Frontiers in Neuroanatomy*, 8:37, 2014.
- [18] Ross Girshick. Fast R-CNN. In *Proceedings of the IEEE International Conference on Computer Vision (ICCV)*, pages 1440–1448, 2015.
- [19] Ross Girshick, Jeff Donahue, Trevor Darrell, and Jitendra Malik. Rich Feature Hierarchies for Accurate Object detection and Semantic Segmentation. In *Proceedings of the IEEE Conference on Computer Vision and Pattern Recognition (CVPR)*, pages 580–587, 2014.
- [20] Lin Gu and Li Cheng. Learning to Boost Filamentary Structure Segmentation. In *Proceedings of the IEEE International Conference on Computer Vision (ICCV)*, pages 639–647, 2015.
- [21] Yanrong Guo, Yaozong Gao, and Dinggang Shen. Deformable MR Prostate Segmentation via Deep Feature Learning and Sparse Patch Matching. *IEEE Transactions on Medical Imaging (TMI)*, 35(4):1077–1089, 2015.
- [22] Jiafa He, Chengwei Pan, Can Yang, Ming Zhang, Yang Wang, Xiaowei Zhou, and Yizhou Yu. Learning Hybrid Representations for Automatic 3D Vessel Centerline Extraction. In *International Conference on Medical Image Computing and Computer-Assisted Intervention (MICCAI)*, pages 24–34. Springer, 2020.
- [23] Ngoc-Vuong Ho, Tan Nguyen, Gia-Han Diep, Ngan Le, and Binh-Son Hua. Point-Unet: A Context-Aware Point-Based Neural Network for Volumetric Segmentation. In *International Conference on Medical Image Computing and Computer-Assisted Intervention (MICCAI)*, pages 644–655. Springer, 2021.

- [24] Ping-Chang Lee, Chao-Chun Chuang, Ann-Shyn Chiang, and Yu-Tai Ching. High-throughput Computer Method for 3D Neuronal Structure Reconstruction from the Image Stack of the *Drosophila* Brain and Its Applications. *PLOS Computational Biology*, 8(9):1–12, 2012.
- [25] Qiufu Li and Linlin Shen. 3D Neuron Reconstruction in Tangled Neuronal Image With Deep Networks. *IEEE Transactions on Medical Imaging (TMI)*, 39(2):425–435, 2019.
- [26] Rongjian Li, Tao Zeng, Hanchuan Peng, and Shuiwang Ji. Deep Learning Segmentation of Optical Microscopy Images Improves 3-D Neuron Reconstruction. *IEEE Transactions on Medical Imaging (TMI)*, 36(7):1533–1541, 2017.
- [27] Cheng Lin, Changjian Li, Yuan Liu, Nenglu Chen, Yi-King Choi, and Wenping Wang. Point2Skeleton: Learning Skeletal Representations from Point Clouds. In *Proceedings of the IEEE/CVF Conference on Computer Vision and Pattern Recognition (CVPR)*, pages 4277–4286, 2021.
- [28] Songtao Liu, Di Huang, and Yunhong Wang. Adaptive NMS: Refining Pedestrian Detection in a Crowd. In *Proceedings of the IEEE/CVF Conference on Computer Vision and Pattern Recognition (CVPR)*, pages 6459–6468, 2019.
- [29] Siqi Liu, Donghao Zhang, Yang Song, Hanchuan Peng, and Weidong Cai. Automated 3-D Neuron Tracing With Precise Branch Erasing and Confidence Controlled Back Tracking. *IEEE Transactions on Medical Imaging (TMI)*, 37(11):2441–2452, 2018.
- [30] Jean Livet, Family A Weissman, Hyuno Kang, Ryan W Draft, Ju Lu, Robyn A Bennis, Joshua R Sanes, and Jeff W Lichtman. Transgenic strategies for combinatorial expression of fluorescent proteins in the nervous system. *Nature*, 450(7166):56–62, 2007.
- [31] Linus Manubens-Gil, Zhi Zhou, Hanbo Chen, Arvind Ramanathan, Xiaoxiao Liu, Yufeng Liu, Alessandro Bria, Todd Gillette, Zongcai Ruan, Jian Yang, et al. BigNeuron: A resource to benchmark and predict best-performing algorithms for automated reconstruction of neuronal morphology. *bioRxiv*, 2022.
- [32] Fausto Milletari, Nassir Navab, and Seyed-Ahmad Ahmadi. V-Net: Fully Convolutional Neural Networks for Volumetric Medical Image Segmentation. In *2016 Fourth International Conference on 3D Vision (3DV)*, pages 565–571. IEEE, 2016.
- [33] Darren R Myatt, Tye Hadlington, Giorgio A Ascoli, and Slawomir J Nasuto. Neuromantic-from semi-manual to semi-automatic reconstruction of neuron morphology. *Frontiers in Neuroinformatics*, 6:4, 2012.
- [34] Hanchuan Peng, Michael Hawrylycz, Jane Roskams, Sean Hill, Nelson Spruston, Erik Meijering, and Giorgio A Ascoli. BigNeuron: Large-Scale 3D Neuron Reconstruction from Optical Microscopy Images. *Neuron*, 87(2):252–256, 2015.
- [35] Hanchuan Peng, Fuhui Long, and Gene Myers. Automatic 3D neuron tracing using all-path pruning. *Bioinformatics*, 27(13):i239–i247, 2011.
- [36] Hanchuan Peng, Zongcai Ruan, Deniz Atasoy, and Scott Sternson. Automatic reconstruction of 3D neuron structures using a graph-augmented deformable model. *Bioinformatics*, 26(12):i38–i46, 2010.
- [37] Olaf Ronneberger, Philipp Fischer, and Thomas Brox. U-Net: Convolutional Networks for Biomedical Image Segmentation. In *International Conference on Medical Image Computing and Computer-Assisted Intervention (MICCAI)*, pages 234–241. Springer, 2015.
- [38] Dong Sui, Kuanquan Wang, Jinseok Chae, Yue Zhang, and Henggui Zhang. A Pipeline for Neuron Reconstruction Based on Spatial Sliding Volume Filter Seeding. *Computational and Mathematical Methods in Medicine*, 2014, 2014.
- [39] Zihao Tang, Donghao Zhang, Yang Song, Heng Wang, Dongnan Liu, Chaoyi Zhang, Siqi Liu, Hanchuan Peng, and Weidong Cai. 3D Conditional Adversarial Learning for Synthesizing Microscopic Neuron Image Using Skeleton-to-Neuron Translation. In *2020 IEEE 17th International Symposium on Biomedical Imaging (ISBI)*, pages 1775–1779. IEEE, 2020.
- [40] Engin Turetken, Fethallah Benmansour, Bjoern Andres, Hanspeter Pfister, and Pascal Fua. Reconstructing Loopy Curvilinear Structures Using Integer Programming. In *Proceedings of the IEEE Conference on Computer Vision and Pattern Recognition (CVPR)*, pages 1822–1829, 2013.
- [41] Dexu Wang, Zhikai Yang, Ziyang Huang, and Lixu Gu. Spine Segmentation with Multi-view GCN and Boundary Constraint. In *2022 44th Annual International Conference of the IEEE Engineering in Medicine & Biology Society (EMBC)*, pages 2136–2139. IEEE, 2022.
- [42] Heng Wang, Yang Song, Zihao Tang, Chaoyi Zhang, Jianhui Yu, Dongnan Liu, Donghao Zhang, Siqi Liu, and Weidong Cai. AI-Enhanced 3D Biomedical Data Analytics for Neuronal Structure Reconstruction. In *Humanity Driven AI*, pages 135–163. Springer, 2022.
- [43] Heng Wang, Yang Song, Chaoyi Zhang, Jianhui Yu, Siqi Liu, Hanchuan Peng, and Weidong Cai. Single Neuron Segmentation Using Graph-Based Global Reasoning with Auxiliary Skeleton Loss from 3D Optical Microscope Images. In *2021 IEEE 18th International Symposium on Biomedical Imaging (ISBI)*, pages 934–938. IEEE, 2021.
- [44] Heng Wang, Chaoyi Zhang, Jianhui Yu, Yang Song, Siqi Liu, Wojciech Chrzanowski, and Weidong Cai. Voxel-Wise Cross-Volume Representation Learning for 3D Neuron Reconstruction. In *Machine Learning in Medical Imaging (MLMI)*, pages 248–257. Springer, 2021.
- [45] Heng Wang, Donghao Zhang, Yang Song, Siqi Liu, Rong Gao, Hanchuan Peng, and Weidong Cai. Memory and Time Efficient 3D Neuron Morphology Tracing in Large-Scale Images. In *2018 Digital Image Computing: Techniques and Applications (DICTA)*, pages 1–8. IEEE, 2018.
- [46] Heng Wang, Donghao Zhang, Yang Song, Siqi Liu, Heng Huang, Mei Chen, Hanchuan Peng, and Weidong Cai. Multiscale Kernels for Enhanced U-Shaped Network to Improve 3D Neuron Tracing. In *Proceedings of the IEEE/CVF Conference on Computer Vision and Pattern Recognition (CVPR) Workshops*, pages 1105–1113, 2019.
- [47] Heng Wang, Donghao Zhang, Yang Song, Siqi Liu, Yue Wang, Dagan Feng, Hanchuan Peng, and Weidong Cai. Segmenting Neuronal Structure in 3D Optical Microscope Images via Knowledge Distillation with Teacher-Student Net-

- work. In *2019 IEEE 16th International Symposium on Biomedical Imaging (ISBI)*, pages 228–231. IEEE, 2019.
- [48] Yu Wang, Arunachalam Narayanaswamy, Chia-Ling Tsai, and Badrinath Roysam. A Broadly Applicable 3-D Neuron Tracing Method Based on Open-Curve Snake. *Neuroinformatics*, 9(2):193–217, 2011.
- [49] Yue Wang, Yongbin Sun, Ziwei Liu, Sanjay E Sarma, Michael M Bronstein, and Justin M Solomon. Dynamic Graph CNN for Learning on Point Clouds. *ACM Transactions on Graphics (TOG)*, 38(5):1–12, 2019.
- [50] Zhirong Wu, Shuran Song, Aditya Khosla, Fisher Yu, Linguang Zhang, Xiaoou Tang, and Jianxiong Xiao. 3D ShapeNets: A Deep Representation for Volumetric Shapes. In *Proceedings of the IEEE Conference on Computer Vision and Pattern Recognition (CVPR)*, pages 1912–1920, 2015.
- [51] Hang Xiao and Hanchuan Peng. APP2: automatic tracing of 3D neuron morphology based on hierarchical pruning of a gray-weighted image distance-tree. *Bioinformatics*, 29(11):1448–1454, 2013.
- [52] Jian Yang, Ming Hao, Xiaoyang Liu, Zhijiang Wan, Ning Zhong, and Hanchuan Peng. FMST: an Automatic Neuron Tracing Method Based on Fast Marching and Minimum Spanning Tree. *Neuroinformatics*, 17(2):185–196, 2019.
- [53] Jianhui Yu, Chaoyi Zhang, Heng Wang, Dingxin Zhang, Yang Song, Tiange Xiang, Dongnan Liu, and Weidong Cai. 3D Medical Point Transformer: Introducing Convolution to Attention Networks for Medical Point Cloud Analysis. *arXiv:2112.04863*, 2021.
- [54] Donghao Zhang, Siqi Liu, Sidong Liu, Dagan Feng, Hanchuan Peng, and Weidong Cai. Reconstruction of 3D neuron morphology using Rivulet back-tracking. In *2016 IEEE 13th International Symposium on Biomedical Imaging (ISBI)*, pages 598–601. IEEE, 2016.
- [55] Ting Zhao, Jun Xie, Fernando Amat, Nathan Clack, Parvez Ahammad, Hanchuan Peng, Fuhui Long, and Eugene Myers. Automated Reconstruction of Neuronal Morphology Based on Local Geometrical and Global Structural Models. *Neuroinformatics*, 9(2):247–261, 2011.

PointNeuron: 3D Neuron Reconstruction via Geometry and Topology Learning of Point Clouds

Supplementary Material

Network Architecture Details

As mentioned in the main paper, our proposed pipeline for the 3D neuron reconstruction task, *PointNeuron*, is composed of two major modules: a skeleton prediction module and a connectivity prediction module. Figure 1 shows the details of our designed network architecture.

The encoder for the neuron point cloud input, based on

DGCNN, has 3 EdgeConv blocks. Each EdgeConv block is used to compute edge features for each point with 20 nearest neighboring points, which has a MLP network $\{c_1, \dots, c_n\}$ where c_i is the number of output channels of the layer i , and a max-pooling layer to generate the locality-aware feature maps. Each MLP layer is followed by a batch normalization and a LeakyReLU activation function with a negative slope of 0.2. These feature maps with multi-scaled

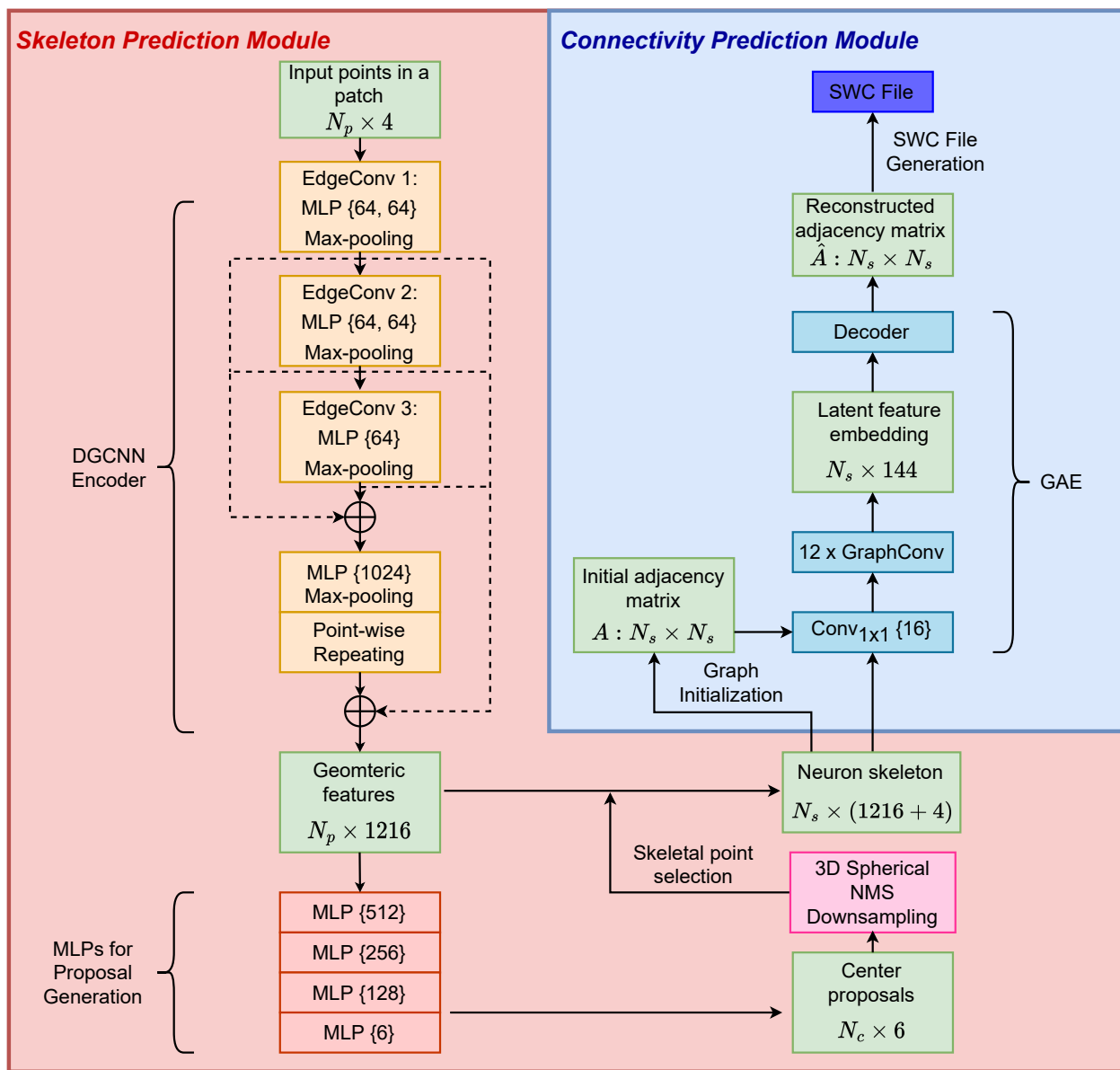


Figure 1: Overall *PointNeuron* architecture. \oplus means the channel-wise concatenation.

receptive fields are concatenated as one through residual connections. As per the main paper, the proposal generation is based on the shared MLP layers to process geometric features, which outputs the center proposals of a 6-channel depth dimension that contains two objectness score values, a radius value, and three XYZ coordinate offset values. The last MLP layer in the proposal generation is not followed by a batch normalization and a ReLU activation function. After 3D spherical NMS downsampling, we could select the skeletal points (or sampled critical center proposals) to constitute the compact neuron skeleton.

The geometric features of skeletal points are concatenated with the point geometric predictions of Cartesian coordinates and radii, which are used as the graph node features in the connectivity prediction module to produce the relationships among skeletal points. The graph adjacency matrix is initialized by a ground truth SWC file when training, or by a traditional tracing algorithm when inferring. Each GraphConv is followed by a batch normalization and a ReLU activation function, and the output feature channels of 12 GraphConv blocks in GAE are $\{32, 32, 48, 64, 64, 80, 96, 96, 102, 128, 128, 144\}$ to compress the node features into the latent embedding. The reconstructed adjacency matrix is obtained through the inner product decoder. In the end, based on the predicted neuron geometric skeleton information and point-wise topology relationships, we design a recursive function to generate the target SWC file.